ACS SENSORS

pubs.acs.org/acssensors

Article

Proton-Only Sensing of Hyperpolarized [1,2-$^{13}C_2$]Pyruvate

Iuliia Mandzhieva, Isaiah Adelabu, Eduard Y. Chekmenev, and Thomas Theis*

Cite This: *ACS Sens.* 2022, 7, 3773−3781

Read Online

ACCESS | Metrics & More | Article Recommendations | Supporting Information

ABSTRACT: Hyperpolarized MRI is emerging as a next-generation molecular imaging modality that can detect metabolic transformations in real time deep inside tissue and organs. ^{13}C-hyperpolarized pyruvate is the leading hyperpolarized contrast agent that can probe cellular energetics in real time. Currently, hyperpolarized MRI requires specialized "multinuclear" MRI scanners that have the ability to excite and detect ^{13}C signals. The objective of this work is the development of an approach that works on conventional (i.e., proton-only) MRI systems while taking advantage of long-lived ^{13}C hyperpolarization. The long-lived singlet state of [1,2-$^{13}C_2$]pyruvate is hyperpolarized with parahydrogen in reversible exchange, and subsequently, the polarization is transferred from the $^{13}C_2$ spin pair to the methyl protons of pyruvate for detection. This polarization transfer is accomplished with spin-lock induced crossing pulses that are only applied to the methyl protons yet access the hyperpolarization stored in the $^{13}C_2$ singlet state. Theory and first experimental demonstrations are provided for our method, which obviates ^{13}C excitation and detection for proton sensing of ^{13}C-hyperpolarized pyruvate with an overall experimental-polarization transfer efficiency of ∼22% versus a theoretically predicted polarization transfer efficiency of 25%.

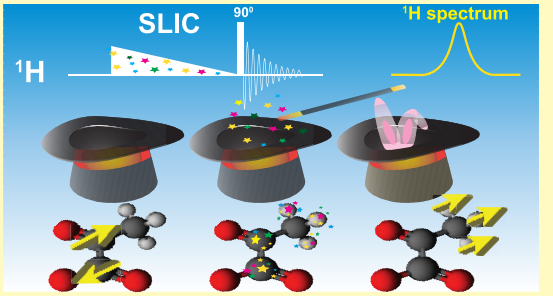

KEYWORDS: *Parahydrogen, hyperpolarization, pyruvate, SABRE, proton sensing, molecular imaging*

NMR hyperpolarization has been developed to create high degrees of nuclear spin polarization approaching order unity compared to a polarization of ∼10^{-5} at thermal equilibrium. As a result, the hyperpolarization process increases magnetic resonance signals by 4−5 orders of magnitude. Hyperpolarized (HP) biologically compatible molecules can be employed as exogenous contrast agents, which enable *in vivo* imaging of metabolic activity.[1−9]

^{13}C-labeled pyruvate is the most promising ^{13}C-hyperpolarized HP contrast agent because it plays a central role in metabolic pathways of cellular energetics. Aberrant HP ^{13}C-pyruvate metabolism has been shown as a potent biomarker for various diseases, such as cancer,[10] diabetes,[11] cardiovascular diseases,[12] and neurological diseases.[13] HP pyruvate is now under evaluation in nearly 40 clinical trials according to clinicaltrials.gov. MRI using HP ^{13}C-pyruvate has the potential to become next-generation molecular imaging because it provides similar metabolic information as ^{18}F-flurodeoxyglucose positron emission tomography (^{18}FDG-PET) scan but with the added benefit of fast (1 min) scan time and operation without ionizing radiation.

Currently, MRI of HP ^{13}C-pyruvate requires full ^{13}C capabilities of an MRI scanner for excitation, slice selection, and detection, which includes specialized RF coils, RF amplifiers, RF chains, and pulse sequences. Only a very few specialized research scanners have this capability out of an estimated 36,000 MRI scanners worldwide. This limitation represents a substantial roadblock for clinical translation of next-generation molecular imaging using HP ^{13}C-pyruvate to routine clinical use.

To solve this translational challenge, one strategy is to transfer HP from ^{13}C nuclei to spin−spin coupled protons[14,15] by pulse sequences such as reverse INEPT.[16−18] This approach has been successfully demonstrated *in vivo* for HP [1-^{13}C]-pyruvate.[19] The key limitation of all previously developed approaches is the requirement to apply RF pulses to the ^{13}C nuclei, which most MRI scanners are not equipped for. Here, we present a new approach for sensing ^{13}C HP pyruvate using an MRI scanner equipped with only standard proton (^{1}H) capabilities. We employ a ^{1}H spin-lock induced crossing (SLIC) pulse to transfer hyperpolarization from a singlet state on the carbons of [1,2-$^{13}C_2$]pyruvate to the methyl protons. The result of such proton excitation is hyperpolarization on the methyl protons, which can be detected by standard ^{1}H RF coils. The presented approach builds on the previous work that has studied polarization transfer in symmetric model spin systems such as $^{13}C_2$-diphenyldiacetyllene using a thermally polarized $^{13}C_2$ singlet order.[20−22]

Received: July 25, 2022
Accepted: November 14, 2022
Published: November 22, 2022

Since then, it has also been shown that the parahydrogen-based hyperpolarization method known as signal amplification by reversible exchange (SABRE) can directly hyperpolarize long-lived singlet states on a variety of substrates,[23−28] including [1,2-$^{13}C_2$]pyruvate.[29,30] SABRE relies on simultaneous exchange of parahydrogen (p-H_2) and to-be-hyperpolarized substrate, *e.g.*, [1,2-$^{13}C_2$]pyruvate studied here.

SABRE is a fast (∼1-minute buildup time) and inexpensive (<$15,000 equipment cost) hyperpolarization method that spontaneously and directly transfers polarization from p-H_2-derived hydrides to nuclear spins of substrate. Here, we employed SABRE to first create an HP $^{13}C_2$ singlet state on [1,2-$^{13}C_2$]pyruvate, followed by a spin-lock induced crossing (SLIC)[21,22,31,32] pulse to transform the HP singlet to NMR-observable proton magnetization on the methyl group. To preserve the $^{13}C_2$ singlet state in $^{13}C_2$ pyruvate, it is necessary to remain at low magnetic fields. Sufficiently low fields preserve the strong coupling regime, where the $^{13}C-^{13}C$ spin−spin-coupling ($^1J_{13C\text{-}13C} \approx 60$ Hz) between the two ^{13}C spins is greater than their chemical shift difference (*i.e.*, the resonance frequency of 1-^{13}C and 2-^{13}C pyruvate spins). In this strong-coupling regime, the singlet state remains close to an eigenstate of the static nuclear spin Hamiltonian. Of note, low field magnets are cheap and do not require expensive cryogens (sometimes in short supply) unlike today's high-field superconducting NMR and MRI scanners. Overall, this work contributes to our long-term goal of improving access to next-generation molecular imaging using the combination of low-field MRI with high-throughput pyruvate hyperpolarization. This combination may establish an affordable molecular imaging platform. In this research article, we demonstrate HP pyruvate sensing using a low-field, 48.5 mT, MRI scanner only using the proton RF chain and pulse sequence without any ^{13}C-related hardware and software. In this paper, we first provide a full theoretical description of polarization transfer from the $^{13}C_2$ pyruvate singlet to methyl protons via a SLIC pulse applied on the proton channel only. Subsequently, we provide the experimental results on a 48.5 mT system to demonstrate the feasibility of this approach even in the presence of large B_1 and B_0 field inhomogeneities.

MATERIALS AND METHODS

Sample Preparation. The catalyst precursor [IrCl(COD)IMes] [COD = cyclooctadiene, IMes = 1,3-bis(2,4,6-trimethylphenyl)-imidazole-2-ylidene] was synthesized as described previously[33] according to the procedure[34,35] described in the literature.

The sample contained 30 mM sodium [1,2-$^{13}C_2$]pyruvate (Sigma-Aldrich-Isotec P/N 493392) as a substrate, 40 mM dimethyl sulfoxide as a co-ligand, and 6 mM catalyst precursor dissolved in methanol-d_4. The samples were prepared by filling 0.5 mL of the stock into standard 5 mm NMR tubes (WG 1000−8, Wilmad), then flushed with argon for 1−2 min to remove oxygen, and sealed under an argon atmosphere.

Experiments. Experimental schematic is shown as Figure 1. The NMR tubes were coupled with a 0.25"-OD Teflon tubing and connected to the Wye connector to the polarizer setup described previously.[36]

The p-H_2 generator described elsewhere[37] was employed to produce 98.5% p-H_2. A mass-flow controller (SmartTrak 50, SierraInstruments) regulated the p-H_2 gas flow with the flow rate set to 70 standard cubic centimeters per minute (sccm). The total p-H_2 pressure in the NMR tube during SABRE experiments was set to 8 bar. Parahydrogen was bubbled through the solution for catalyst activation[38,39] at 25 °C for 15 min before any experiments. During the catalyst activation period, the solution changed the color from yellow to clear.

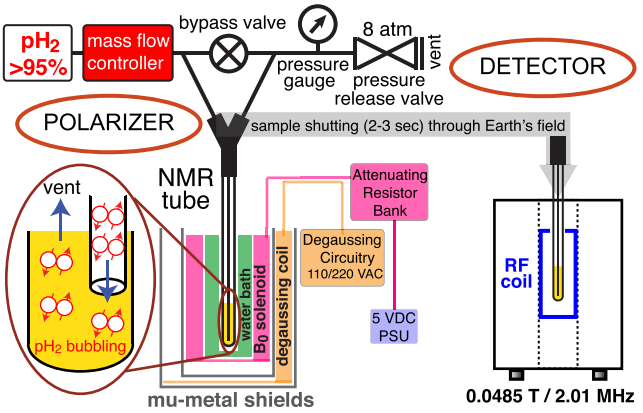

Figure 1. Experimental schematic for performing SABRE-SHEATH hyperpolarization followed by sample transfer and proton-only sensing of hyperpolarized [1,2-$^{13}C_2$]pyruvate at ∼2 MHz.

Hyperpolarization of the $^{13}C_2$ Singlet State of [1,2-$^{13}C_2$]Pyruvate. SABRE-SHEATH (signal amplification by reversible exchange in shield enables alignment transfer to heteronuclei) experiments were conducted in a μ-metal shield (three layers, ZG-209, Magnetic Shield Corp.). The degaussing circuitry employed here was described previously.[36] The required magnetic field in the μT regime is generated by a small coil inside the shield after proper degaussing.[36] 1/16" OD, 1/32" ID Teflon tubing was submerged in the solution.

We hyperpolarized sodium [1,2-$^{13}C_2$]pyruvate by pressurizing the NMR tube to an 8 bar total p-H_2 pressure, followed by p-H_2 bubbling for 60 s with the flow rate set to 150 sccm at 1.7 μT.

As soon as the p-H_2 flow was turned off, the sample was transferred to 48.5 mT for detection (2−4 s time delay between cessation of p-H_2 flow and initiation of polarization transfer sequence).

The low magnetic field was generated by a permanent magnet configured in a Halbach array with B_0 = 48.5 mT (Magritek, Wellington, New Zealand).

A RF multiturn solenoid coil was used for the pulse application on the ^1H channel.[40] The NMR probe frequency was 2.01905 MHz. The ramped SLIC pulse was implemented as described previously.[41,42]

Simulations. The spin evolution was simulated using SPINACH[43] simulation library version 2.6.5625 in MATLAB (R2021a) as described below. We explore two different approaches to perform SLIC experiments, for both the 3-spin system ($^{13}C_2$ pair and one proton) and for the 5-spin system ($^{13}C_2$ pair and CH_3), namely, square SLIC pulses and adiabatic linear B_1 ramps. Both cases were simulated for on-resonance and off-resonance ^1H-SLIC irradiation. The off-resonance case is important to consider because of the experimental B_0 inhomogeneities, whereas the adiabatic B_1 ramps are implemented to compensate for experimental B_1 inhomogeneities. Table 1 lists all the J-coupling and chemical shift parameters that were used to construct the respective spin Hamiltonians.

RESULTS AND DISCUSSIONS

As displayed in Figure 2a, to hyperpolarize the singlet state of [1,2-$^{13}C_2$]pyruvate, we use SABRE-SHEATH, where p-H_2 and substrate reversibly bind to a Ir-IMes-based polarization

Table 1. Summary of Chemical Shifts and Spin−Spin Couplings Used in the Simulations

chemicalshift [ppm]	^1H	2-^{13}C	1-^{13}C	
	0	30	0	
J-coupling [Hz]	$^1H-^1H$	2-$^{13}C-^1H$	1-^{13}C-^1H	$^{13}C-^{13}C$
	15	−4.76	1.62	61

https://doi.org/10.1021/acssensors.2c01608
ACS Sens. 2022, 7, 3773−3781

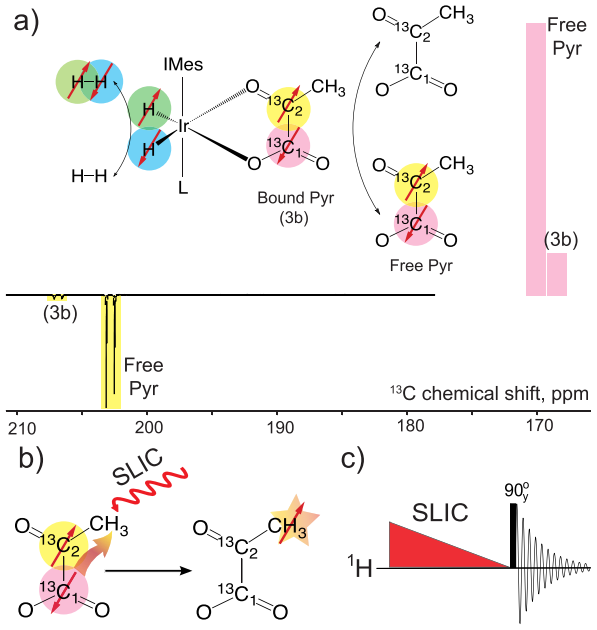

Figure 2. (a) The SABRE process enables spontaneous transfer of *p*-H_2–derived hydride singlet spin order to overpopulate the $^{13}C_2$ nuclear spin singlet of the [1,2-$^{13}C_2$]pyruvate substrate through a spin–spin coupling network of the catalyst-bound state (**3b**); the reversible substrate exchange leads to substrate release and formation of free substrate. The resulting ^{13}C spectrum (9.4 T) reveals the presence of an HP $^{13}C_2$ pyruvate singlet as two anti-phase resonances; note the signatures of free and catalyst bound (**3b**) species. (b) SLIC pulse applied only on the proton channel drives polarization from the $^{13}C_2$ pyruvate singlet to methyl protons. (c) Pulse sequence for linear ramp SLIC pulse for polarization transfer and ^{1}H signal detection at 48.5 mT.

transfer complex (PTC).[34,35] The hyperpolarization is transferred from *p*-H_2-derived hydrides to the $^{13}C_2$ spins, specifically targeting singlet order by selection of the ideal field. The substrate is in reversible exchange, and a pool of free HP pyruvate is created in the solution over time (tens of seconds). At the appropriate magnetic field, B_0, 1.7 μT in this case, the $^{13}C_2$ singlet state is overpopulated spontaneously.

As detailed previously,[23,30,44] there are two resonance conditions for the singlet order creation:

$$J_{CC'} = \pm J_{HH'} \tag{1}$$

and

$$B_0 = \frac{J_{HH'} + J_{CC'}}{\gamma_{1H} - \gamma_{13C}} \tag{2}$$

where $J_{CC'}$denotes spin–spin coupling between 1-^{13}C and 2-^{13}C of [1,2-$^{13}C_2$]pyruvate, γ_{1_H} and γ_{13_C} are the ^{1}H and ^{13}C gyromagnetic ratios, respectively, while $J_{HH'}$ denotes the spin–spin coupling between hydride spins. In the present case, $J_{CC'}\approx$ 60 Hz in the catalyst bound state and $J_{HH'}\approx -10.6$ Hz. Therefore, the first resonance has significantly reduced efficiency, and indeed, we primarily rely on the second to generate polarization transfer. Experimentally, we obtain the best hyperpolarization level of the singlet order by adjusting the magnetic field to 1.7 μT, while the equation above predicts 1.55 μT. The difference between experiment and analytical solution is likely due to experimental offsets in the residual magnetic field inside the magnetic shields. Full details of hyperpolarizing distinct spin states in the [1,2-$^{13}C_2$]pyruvate will be provided elsewhere.

To prove the creation of the the $^{13}C_2$ singlet state, we transferred the sample to a high field (9.4 T) NMR and detected a standard 1D NMR spectrum with a 90° excitation pulse, displayed in Figure 2a. The observed antiphase spectrum of 1-^{13}C and 2-^{13}C resonances proves that the two ^{13}C spins indeed formed a singlet state: the 1-^{13}C peak appears at 170 ppm, and the 2-^{13}C peak resonates at 203 ppm pointing in opposite directions; note the presence of free and bound (**3b**) species (the **3b** naming convention is based on the original publication discussing these systems[29]).

Once the $^{13}C_2$ singlet state is hyperpolarized, the second step, which we describe in full detail here, is the transfer of hyperpolarization to the CH_3 group via SLIC.

Figure 2b illustrates the general effect of an SLIC pulse applied on the ^{1}H channel at the methyl protons' frequency using a 48.5 mT magnet.[40,45] The SLIC pulse drives the polarization from the overpopulated $^{13}C_2$ singlet to methyl protons, where it is detected without ever using ^{13}C RF irradiation.

Figure 2c shows the experimental implementation where we used a SLIC pulse with a linear ramp of B_1 strength. The linear ramp was employed to compensate for severe experimental B_1 and B_0 inhomogeneities of the employed 48.5 mT scanner.

Before analysis of the experimental results, we discuss the underlying theory. For this purpose, we simplify the spin system by noting that the three pyruvate methyl protons are magnetically equivalent, and so we first reduce the system to a three-spin system (consisting of 1-^{13}C, 2-^{13}C, and ^{1}H) by replacing the $-CH_3$ motif with a single ^{1}H. This analysis yields 8 × 8 matrices instead of 32 × 32 matrices. Further below, we provide full simulations on the complete five-spin system (consisting of 1-^{13}C, 2-^{13}C, and three methyl protons).

The analysis begins with the general Hamiltonian of the three-spin system at hand, given as

$$H_{3-\text{spin}} = \nu_C(I_{1z} + I_{2z}) + \nu_H S_z + J_{CC'} I_1 \cdot I_2 + \frac{|J_{C'H} - J_{CH}|}{2} (I_1 \cdot S - I_2 \cdot S) + \frac{J_{C'H} + J_{CH}}{2}(I_1 \cdot S + I_2 \cdot S) \tag{3}$$

where ν_C is the ^{13}C resonance frequency, ν_H is the proton resonance frequency, $\boldsymbol{I}_1$ and $\boldsymbol{I}_2$ are the spin operators for 1-^{13}C and 2-^{13}C, while $\boldsymbol{S}$ is the spin operator representing ^{1}H, I_{1z} and I_{2z} are the z-components of $\boldsymbol{I}_1$ and $\boldsymbol{I}_2$, and J_{CC} denotes the ^{13}C–^{13}C spin–spin coupling. $J_{C'H}$ and J_{CH} are spin–spin coupling between 1-^{13}C and ^{1}H and 2-^{13}C and ^{1}H, respectively.

For ease of mathematical analysis, it is also useful to introduce the sum and difference terms of the out-of-pair couplings as

$$\Delta J_{CH} = |J_{C'H} - J_{CH}| \tag{4}$$

and

$$\Sigma J_{CH} = J_{C'H} + J_{CH} \tag{5}$$

If we apply an RF pulse along the x-direction on resonance with the single proton, we can formulate the RF Hamiltonian as follows.

$$H_{RF} = B_1 \times S_x \tag{6}$$

https://doi.org/10.1021/acssensors.2c01608
ACS Sens. 2022, 7, 3773–3781

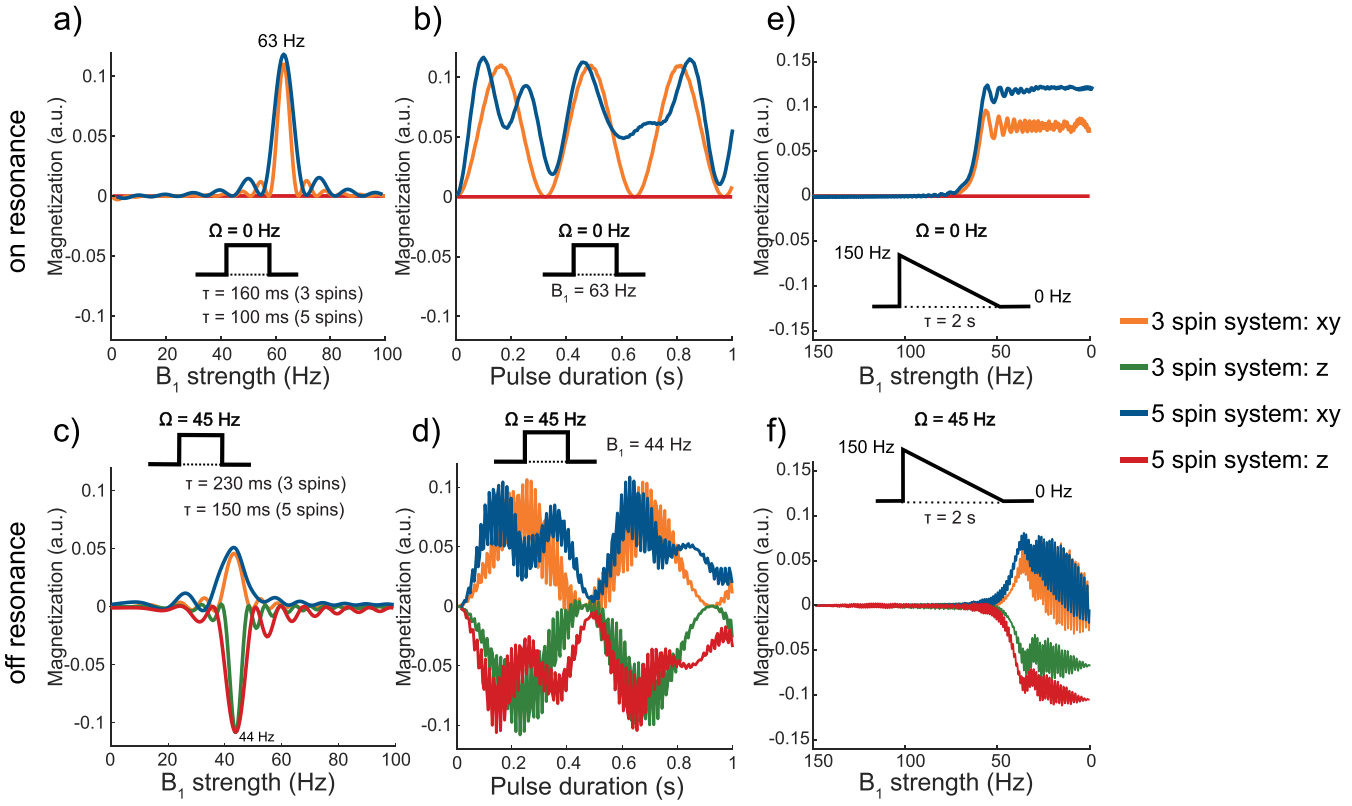

Figure 3. Simulated ^{1}H magnetization intensity after application of a SLIC pulses to singlet-hyperpolarized [1,2-$^{13}C_2$]pyruvate. In all graphs, *z*-magnetization and transverse (*xy*) magnetization are shown for the three- and five-spin systems. (a) ^{1}H magnetization as a function of B_1 strength of a square SLIC pulse of 160 (for the three-spin system) and 100 ms (for the five-spin system) applied on resonance (frequency offset Ω^0 = 0 Hz); (b) ^{1}H magnetization as a function of pulse duration of a square SLIC pulse with B_1 = 63 Hz on resonance (frequency offset Ω^0 = 0 Hz); (c) ^{1}H magnetization as a function of B_1 strength of an off resonance (frequency offset Ω^0 = 45 Hz), square SLIC pulse with 230 (three-spin system) and 150 ms (five-spin system) duration; (d) ^{1}H magnetization as a function of pulse duration of a square, off resonance (Ω^0 = 45 Hz) SLIC pulse with a B_1 strength amplitude of 44 Hz; (e) ^{1}H magnetization as a function of B_1 strength of a linearly ramped pulse with an initial signal amplitude of 150 Hz on resonance (Ω^0 = 0 Hz) and a duration of 2 s; (f) ^{1}H magnetization as a function of B_1 strength of a linearly ramped pulse linear with an initial signal amplitude of 150 Hz off resonance (frequency offset Ω^0 = 45 Hz).

where B_1 is the amplitude of the applied RF pulse. Therefore, the total nuclear spin Hamiltonian can be expressed as

$$H_{\text{total}} = \nu_C(I_{1z} + I_{2z}) + \nu_H S_z + J_{CC} I_1 \cdot I_2 + \frac{\Delta J_{CH}}{2}(I_1 \cdot S - I_2 \cdot S) + \frac{\Sigma J_{CH}}{2}(I_1 \cdot S + I_2 \cdot S) + \gamma_{1H} B_1 \cdot S_x \quad (7)$$

As we will show in the following, in the case of on resonance RF, efficient hyperpolarization transfer from the $^{13}C_2$ singlet state to the methyl proton is possible if the B_1 matches the J_{CC}

To further aid analysis, it is also helpful to employ the singlet−triplet basis to describe the $^{13}C_2$ spin states, whereas for the ^{1}H proton, we use quantization along $-x$ and $+x$ directions, where

$$|x_-\rangle = \frac{1}{\sqrt{2}}(|\alpha\rangle - |\beta\rangle),\ |x_+\rangle = \frac{1}{\sqrt{2}}(|\alpha\rangle + |\beta\rangle) \quad (8)$$

Combining ^{13}C and proton states results in 4 × 2 = 8 total spin states (for example, $|S_0 x_+\rangle$). The matrix representation of the full spin 8×8 Hamiltonian is given in the Supporting Information (SI), while here, we focus on the part of the total Hamiltonian that illustrates population transfer from $|S_0 x_+\rangle$ to $|T_0 x_-\rangle$. For physical interpretation, we note that before applying the SLIC pulse, there is no ^{1}H polarization. Proton polarization along B_1 is created by inducing population transfer between these two states. The relevant subspace in the matrix representation of the Hamiltonian is

$$\begin{array}{c} \\ |S_0 x_+\rangle \\ |T_0 x_-\rangle \end{array} \begin{array}{c} \begin{array}{cc} |S_0 x_+\rangle & |T_0 x_-\rangle \end{array} \\ \begin{pmatrix} \frac{B_1}{2} - \frac{3}{4}J_{CC} & \frac{\Delta J_{CH}}{4} \\ \frac{\Delta J_{CH}}{4} & -\frac{B_1}{2} + \frac{1}{4}J_{CC'} \end{pmatrix} \end{array} \quad (9)$$

This matrix indicates that ΔJ_{CH} can drive population transfer, when the difference between diagonal elements in this part of Hamiltonian vanishes. Therefore, if

$$\frac{B_1}{2} - \frac{3J_{CC}}{4} = -\frac{B_1}{2} + \frac{J_{CC}}{4} \quad (10)$$

then the off-diagonal elements can take full effect and rotate the population from $|S_0 x_+\rangle$ to$|T_0 x_-\rangle$. This analysis establishes the resonance condition.

$$B_1 = J_{CC} \quad (11)$$

https://doi.org/10.1021/acssensors.2c01608
ACS Sens. 2022, 7, 3773−3781

So, if the B_1power matches J_{CC} and if it is applied on resonance, then polarization can be transferred to the spin−spin-coupled proton. This analysis is accurate for a three-spin system and on-resonance RF. The actual experiments are on a five-spin system with a CH_3 group and suffer from B_1 and B_0 inhomogeneities. In order to understand the effect of additional spins as well as RF offsets, we performed spin dynamics simulations for these more complicated scenarios detailed in the following.

In the simulations, the initial density matrix was the $^{13}C_2$-pyruvate singlet, followed by sample transfer from the μT field (where the singlet order is generated) to the 48.5 mT field, where polarization transfer via SLIC and signal detection occurs. The details of this process are described in the SI. The resulting density matrix was evolved under the Hamiltonian of the system including the RF-irradiation at 48.5 mT. Square SLIC pulses were encoded with x phase on the ^{1}H channel with specified duration. No additional pulses were simulated after the SLIC pulse. Simply, the magnetization in the transverse plane $L_+ = (L_x + iL_y)/2$ on the proton(s) or magnetization along z is computed at the end of the SLIC pulses and plotted in Figure 3.

Figure 3 shows the simulations of the most important features of the three-spin and five-spin systems under SLIC irradiation. Specifically, effects of B_1 power, pulse duration, shape, and off-resonance irradiation are analyzed for the two different spin systems. Figure 3a examines polarization transfer from the $^{13}C_2$ singlet state to ^{1}H as a function of B_1 power at the on-resonance condition (frequency offset $\Omega^0 = 0$). For both the three-spin and the five-spin system, maximum transfer occurs at $B_1 = 63$ Hz, corresponding to the resonance condition equation derived from eq 11:

$B_1 = 63$ Hz $\approx J_{CC'} = 61$ Hz. The reason for the 2 Hz difference between analytical and simulated outcomes is that there is a slight frequency difference between the two carbons at 48.5 mT, which is not taken into account in the analytical model but is included in the simulations ($\Delta\delta = 30.1$ ppm = 15.6 Hz@ 48.5 mT). Both spin systems show a maximum transfer efficiency at the same B_1 strength of 63 Hz.

Figure 3b shows all the magnetization terms as a function of pulse duration. With on-resonance irradiation with $B_1 = 63$ Hz, no z-magnetization is formed. Interestingly, the five-spin system, with the CH_3 group reaches the maximum faster; after only 100 ms the first maximum is achieved, whereas in the three-spin system the maximum does not appear until 165 ms.

Also, the three-spin system shows simple sinusoidal oscillations, whereas the five-spin system displays a more irregular pattern.

As depicted in Figure 3c, once we take a SLIC pulse frequency offset into account, magnetization along the z-direction is formed. We chose an RF-offset of $\Omega = 45$ Hz to illustrate these effects. With this offset, we calculate the magnetization along z as well as in the transverse plane (xy) as a function of B_1 power. As illustrated, all magnetization terms reach a maximum at a B_1 power of 44 Hz, where more magnetization is along z compared to transverse (xy). For this simulation, the pulse length was chosen at 160 ms because this value provides the maximum polarization transfers under this off-resonance condition, as illustrated in Figure 3d. This figure also shows that off-resonance effects induce much more rapid oscillations and complicate the control over the polarization transfer process. In this sense, Figure 3d illustrates the challenges caused by both B_0 and B_1 inhomogeneities. The simulated behavior indicates that exact control over B_1 and B_0 is necessary to achieve good polarization transfer; however, this is experimentally challenging in our nonoptimized setup employed and detailed below.

Because of the potential experimental limitations, we have designed linearly ramped B_1 pulses, which impart robustness toward B_1 and B_0 inhomogeneities. The linear ramp approach allows for adiabatic sweep through the resonance conditions that are spread across the sample because of the inhomogeneities. The slow sweep allows for excitation of the dispersed resonances as the B_1 is reduced slowly.

In the simulation, the B_1 amplitude goes from 150 to 0 Hz during 2 s. Figure 3e,f displays the various magnetization terms (z, xy) during the pulse on resonance ($\Omega = 0$ Hz) and off-resonance ($\Omega = 45$ Hz), respectively. Figure 3e illustrates that xy-magnetization appears when the B_1 pulse amplitude approaches 80 Hz and reaches a plateau toward the end of the pulse. At the end of this ramped pulse, xy-magnetizations were similar to values obtained from square pulses. In analogy to the effects observed for the square SLIC pulse (Figure 3a,b), no z-magnetization was formed for the on-resonance case for the adiabatic (ramped) pulse (Figure 3e). In addition, we simulated the off-resonance effects (frequency offset $\Omega = 45$ Hz) for the adiabatic pulse (Figure 3f). Again, once the B_1 pulse amplitude reaches ∼80 Hz, the off-resonance effects transform xy-magnetization to z-magnetizations for both three- and five-spin systems. Simulated effects of square and adiabatic pulses allow us to conclude that in experiments with B_0 and B_1 inhomogeneities (off-resonance case), we primarily expect to observe z-magnetization.

Based on these detailed simulations, we proceeded to experimental implementation to demonstrate polarization transfer from the $^{13}C_2$-pyruvate singlet to the methyl protons via adiabatic SLIC pulses applied at the ^{1}H channel only.

First, the $^{13}C_2$ pyruvate singlet was hyperpolarized in a magnetic shield by SABRE-SHEATH.[46,47] The maximum singlet state polarization on the $^{13}C_2$ spin pair was achieved at 1.7 μT. The field dependence is illustrated in the Supporting Information. As shown in the event sequence, illustrated in Figure 4a, after hyperpolarizing the $^{13}C_2$ singlet state, we manually transferred the sample from the shield to a low-field imaging system ($B_0 = 48.5$ mT). This 48.5 mT system employed in these proof-of-concept demonstrations suffers from significant B_1 and B_0 inhomogeneities, which stem from nonideal arrangements of the permanent magnet arrays and poor matching of the B_1 coils to our sample size. These inhomogeneities complicated our experimental efforts because, as demonstrated in the simulations above, square SLIC pulses are exquisitely sensitive to B_1 power, pulse duration, and off-resonance effects. Therefore, we implemented the adiabatically ramped shapes that are more immune to these imperfections.

After the optimizations (detailed below), we obtained the spectrum shown in Figure 4b. As it can be seen, the frequency range of HP resonance spans over almost 200 Hz, characterizing the significant nonidealities of this system. Of note, the intensity "burn-out" in the middle of spectrum has zero frequency offset. This intensity depression can be rationalized with the simulations provided in Figure 3e, which shows that exact on-resonance irradiation only produces xy-magnetization, which is prone to dephasing and is not detected after the 90° excitation pulse used in our experiments. In contrast, the off-resonance components of the SLIC pulse produce z-magnetization as indicated in Figure 3f. The near-zero-offset signal

https://doi.org/10.1021/acssensors.2c01608
ACS Sens. 2022, 7, 3773−3781

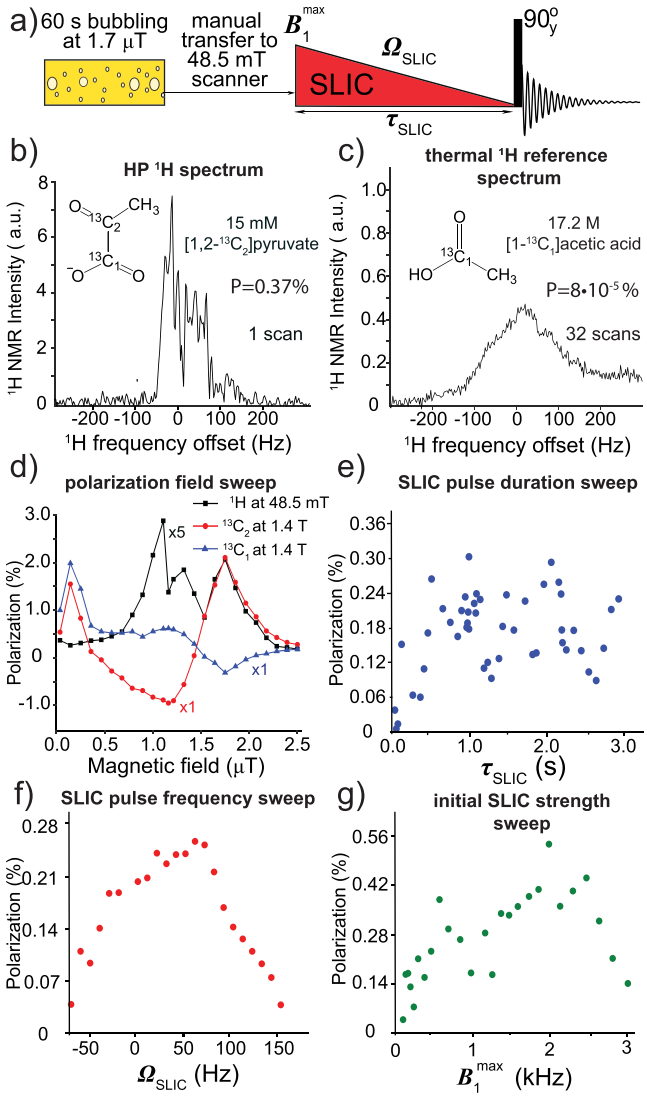

Figure 4. (a) Schematic of the experiment with SLIC pulse for polarization transfer from HP $^{13}C_1$–$^{13}C_2$ singlet to methyl protons of [1,2-$^{13}C_2$]pyruvate. (b) ^{1}H spectrum acquired after SLIC pulse with 2.01905 MHz frequency and 1 s duration at 12 °C and 48.5 mT; (c) ^{1}H spectrum of thermally polarized reference pure 17.2 M [1-$^{13}C_1$]acetic acid at 48.5 mT; (d) Magnetic field sweep of [1,2-$^{13}C_2$]pyruvate polarization at 12 °C. ^{13}C polarization was detected at 1.4 T, whereas ^{1}H polarization was detected at 48.5 mT after a SLIC pulse; (e) pulse duration sweep acquired using a SLIC pulse with a 2.0905 MHz frequency and B_1(max) = 1953 Hz as the initial amplitude; (f) frequency sweep acquired after SLIC pulse with B_1(max) = 1953 Hz as the initial pulse amplitude with a 2 s duration. (g) Power sweep acquired after an SLIC pulse with a 2.01905 MHz frequency and 1 s duration.

depression supports our theoretical simulations. Spin evolution with a frequency offset generates z-magnetization that is converted into detectable signal with the hard 90° pulse and observed in the spectrum shown in Figure 4b.

We used thermally polarized pure [1-^{13}C]acetic acid as signal reference to calculate polarization levels achieved in [1,2-$^{13}C_2$]pyruvate at 48.5 mT (Figure 4c) and at 1.4 T (see Figure S3, SI). Note that the hyperpolarized signal is 11.8 times larger than the thermal signal, which would constitute ^{1}H background in an application with highly concentrated protons in the solvent.

We performed a series of control experiments to confirm that the observed signal corresponds to the implementation of SLIC pulses. First, we applied only a hard 90° pulse and we did not observe ^{1}H signal (see SI). Second, we applied an SLIC pulse with 0 Hz amplitude followed by a hard 90° pulse and we did not observe any signal (see Figure S10).

To confirm that the SLIC-induced proton signal originates from the $^{13}C_2$ singlet, we performed magnetic field sweep experiment for ^{1}H signal (detection at 48.5 mT) and ^{13}C signals (detection at 1.4 T) of [1,2-$^{13}C_2$]pyruvate displayed in Figure 4d. Specifically, we varied the microtesla magnetic field, at which we bubbled p-H_2 to create an overpopulated $^{13}C_2$ singlet. Indeed, the field sweep profile of ^{1}H signal detected at 48.5 mT after SLIC pulse matches remarkably well to the field profile of ^{13}C signal detected at 1.4 T right after p-H_2 bubbling, supporting our claim that the proton signal detected at 48.5 mT indeed originates from the $^{13}C_2$ singlet. For example, the two ^{1}H maxima seen at 1.0 and 1.7μT coincide with the maxima observed for the $^{13}C_2$ singlet, identified by the largest amplitude differences between 1-^{13}C and 2-^{13}C in the 1.4 T ^{13}C spectra.

We experimentally characterized the behavior of the system as a function of pulse duration (Figure 4e), irradiation frequency (Figure 4f), and B_1 SLIC pulse strength (Figure 4g). Specifically, we employed a linearly ramped SLIC pulse ramping from high B_1 (above the resonance condition (B_1 = J_{CC} ≈ 60 Hz) down to 0 as shown on Figure 4a.

Based on the first optimization, concerning the initial B_1 power, we proceeded with the exploration of pulse duration. Here, we used an initial B_1 pulse amplitude of ∼2 kHz and a frequency of 2.01905 MHz (optimal parameter set from Figure 4g). The results are depicted in Figure 4e, where we observe pronounced oscillations of the signals, which are rationalized by comparing to the simulations in Figure 3d,f. The latter shows that the spins that are off-resonance due to B_0 inhomogeneities will exhibit strong oscillations as a function of pulse duration.

Finally, a frequency sweep was performed to investigate the effect of the overall frequency offset on the detected signal (Figure 4f). The SLIC pulse frequency was swept across a 200 Hz window centered at 2.019100 MHz, *i.e.*, from 2,019,000 to 2,019,200 Hz. We chose a pulse duration of 1 s and an initial B_1 amplitude of 2 kHz. As it can be seen, the width of the observed feature matches the frequency distribution of the spins in the spectrum. This behavior can be rationalized because the ideal SLIC performance requires SLIC pulse irradiation very close to the on-resonance condition, and in this case, the frequency distributions due to B_0 inhomogeneities dominate.

To explore the effects of the adiabatic pulse slope, we varied the initial B_1 strength from 3 kHz to 0 Hz while maintaining a pulse duration of 1 s and an SLIC RF-frequency of 2.01905 MHz, which is on-resonance for the center of the detected signal (Figure 4g).

Figure 4g shows no signal when the initial pulse amplitude is less than 20 Hz or more than 2500 Hz while keeping in mind that a distribution of B_1 values exists across the sample. In this present setup, the signal is maximized by starting the pulse at a relatively large amplitude, which is well above the resonance condition ((B_1 = J_{CC} ≈ 60 Hz) everywhere in the sample and then reducing the B_1 power slowly.

We have determined the maximum observed efficiency of polarization transfer (χ) of our procedure by dividing the

https://doi.org/10.1021/acssensors.2c01608
ACS Sens. 2022, 7, 3773−3781

experimentally measured maximum P_H of 0.56% (Figure 4g), measured after polarization transfer by $^{13}C_2$-singlet polarization of 2.5% (Figure 4d) measured before polarization transfer (see SI for analysis). The magnetic field in the shields was 1.7 μT. The highest value of experimentally observed polarization transfer efficiency χ was 22% (typical χ values in our experiments were ~0.3/2.5 × 100 = 12%), whereas the theoretical limit of this transfer efficiency is 25% as determined by our simulations (see SI for details on these calculations; also, see ref 48).

Optimization of the experimental setup and RF pulses can be expected to increase the experimental polarization transfer efficiency closer to the theoretical limit.

In the Supporting Information, we provide a detailed theoretical analysis that shows how to differentiate pyruvate from lactate signal as a likely metabolic product of pyruvate. In brief, conversion to lactate introduces a strongly coupled proton onto the $^{13}C_2$ spin pair. This interaction can be suppressed by decoupling until the desired time of detection. At that time, decoupling is stopped and the singlet state on lactate can be converted to ^{1}H polarization with a much shorter and weaker SLIC pulse that does not affect the pyruvate singlet state. Thereafter, the developed SLIC pulses shown here can be employed to read out the pyruvate. In this manner, it becomes feasible to acquire separated lactate and pyruvate signals. Complete simulations of this envisioned scheme are provided in the SI.

Finally, we note that the hyperpolarized signals at 48.5 mT typically exceed the thermal polarization of the background signal by at least 10-fold. Nonetheless, the SI also provides a SLIC pulse strategy that suppresses the background signal entirely, which works by placing the background signal along z at the end of the SLIC pulse such that only hyperpolarized signal is detected.

CONCLUSIONS

In summary, we presented an approach that transfers polarization from the $^{13}C_2$-singlet state of [1,2-$^{13}C_2$]pyruvate to methyl pyruvate protons using the proton channel-only of a low-field MRI scanner. This technique allows the combination of the benefits of hyperpolarization methods and long ^{13}C-polarization lifetimes with MRI scanners that only have ^{1}H channels. The polarization transfer is accomplished with spin-lock induced crossing (SLIC) pulses that are applied only to the methyl protons of [1,2-$^{13}C_2$]pyruvate, even though the hyperpolarization is stored in the $^{13}C_2$ singlet state. In this paper, we detailed the theoretical analysis of this polarization transfer scheme and provided first proof-of-concept experimental evidence. In both simulations and experiments, we explored effects of SLIC pulse duration, B_1 power, and frequency. First, we provided analytical insights for a three-spin system, followed by numerical solutions for three- and five-spin systems, which provide insight into the underlying spin dynamics. The pilot experiments presented employed a nonoptimized setup with severe B_1 and B_0 inhomogeneities of a 48.5 mT scanner. Despite these limitations, the experimental results agreed with the theoretical analysis. In future applications, the 22% experimentally observed polarization transfer efficiency may be improved by using magnet systems with more homogeneous fields or by advanced design of other RF pulse sequences that may be less susceptible to experimental imperfections.[22,49] A strategy to differentiate multiple metabolites, e.g., pyruvate and lactate, as well as a strategy to suppress background signal, is detailed in the Supporting Information. The presented method can likely be expanded to other metabolically relevant molecules with similar spin systems such as α-ketoglutarate—experiments in progress in our laboratories.

ASSOCIATED CONTENT

Supporting Information

The Supporting Information is available free of charge at https://pubs.acs.org/doi/10.1021/acssensors.2c01608.

Additional details, materials, and methods, including experiments and computer simulations (PDF)

AUTHOR INFORMATION

Corresponding Author

Thomas Theis − *Department of Chemistry and Department of Physics, North Carolina State University, Raleigh, North Carolina 27606, United States; Joint Department of Biomedical Engineering, University of North Carolina at Chapel Hill and North Carolina State University, Raleigh, North Carolina 27695, United States;* orcid.org/0000-0001-6779-9978; Email: ttheis@ncsu.edu

Authors

Iuliia Mandzhieva − *Department of Chemistry, North Carolina State University, Raleigh, North Carolina 27606, United States;* orcid.org/0000-0001-9154-9012

Isaiah Adelabu − *Department of Chemistry, Wayne State University, Detroit, Michigan 48202, United States*

Eduard Y. Chekmenev − *Department of Chemistry and Biosciences (Ibio), Wayne State University, Detroit, Michigan 48202, United States; Karmanos Cancer Institute (KCI), Detroit, Michigan 48201, United States;* orcid.org/0000-0002-8745-8801

Complete contact information is available at: https://pubs.acs.org/10.1021/acssensors.2c01608

Notes

The authors declare the following competing financial interest(s): The authors declare the following competing financial inter-est(s): Thomas Theis holds stock in Vizma Life Sciences LLC (VLS) and is President of VLS. VLS is developing products related to the research being reported. The terms of this arrangement have been reviewed and approved by NC State University in accordance with its policy on objectivity in research. The authors have filed a provisional patent application through NC State University with the USPTO regarding this work (Application # 63/203,591). EYC discloses a stake of ownership in XeUS Technologies, LTD.

ACKNOWLEDGMENTS

Research reported in this publication was supported by the National Institute of Biomedical Imaging and Bioengineering of the National Institutes of Health under award nos. NIH R21EB025313 and NIH R01EB029829. The content is solely the responsibility of the authors and does not necessarily represent the official views of the National Institutes of Health. In addition, we acknowledge funding from the Mallinckrodt Foundation, the National Science Foundation under award no. NSF CHE-1904780, the National Cancer Institute under award no. NCI 1R21CA220137, and the North Carolina Biotechnology Center in the form of a Translational Research

Grant. Finally, we would like to acknowledge the support from NCSU's METRIC providing access to NMR instrumentation.

■ ABBREVIATIONS

HP, hyperpolarization; SLIC, spin-lock induced crossing

■ REFERENCES

(1) Wang, Z. J.; Ohliger, M. A.; Larson, P. E. Z.; Gordon, J. W.; Bok, R. A.; Slater, J.; Villanueva-Meyer, J. E.; Hess, C. P.; Kurhanewicz, J.; Vigneron, D. B. Hyperpolarized ^{13}C MRI: State of the Art and Future Directions. *Radiology*. **2019**, 273−284.

(2) Gallagher, F. A.; Kettunen, M. I.; Hu, D.-E.; Jensen, P. R.; Zandt, R. I.; Karlsson, M.; Gisselsson, A.; Nelson, S. K.; Witney, T. H.; Bohndiek, S. E.; Hansson, G.; Peitersen, T.; Lerche, M. H.; Brindle, K. M. Production of hyperpolarized [1,4-13C2]malate from [1,4-13C2]fumarate is a marker of cell necrosis and treatment response in tumors. *Proc. Natl. Acad. Sci. U. S. A.* **2009**, *106*, 19801−19806.

(3) Wilson, D. M.; Keshari, K. R.; Larson, P. E. Z.; Chen, A. P.; Hu, S.; van Criekinge, M.; Bok, R.; Nelson, S. J.; MacDonald, J. M.; Vigneron, D. B.; Kurhanewicz, J. Multi-Compound Polarization by DNP Allows Simultaneous Assessment of Multiple Enzymatic Activities in Vivo. *J. Magn. Reson.* **2010**, *205*, 141−147.

(4) Nelson, S. J.; Kurhanewicz, J.; Vigneron, D. B.; Larson, P. E. Z.; Harzstark, A. L.; Ferrone, M.; van Criekinge, M.; Chang, J. W.; Bok, R.; Park, I.; Reed, G.; Carvajal, L.; Small, E. J.; Munster, P.; Weinberg, V. K.; Ardenkjaer-Larsen, J. H.; Chen, A. P.; Hurd, R. E.; Odegardstuen, L.-I.; Robb, F. J.; Tropp, J.; Murray, J. A. Metabolic Imaging of Patients with Prostate Cancer Using Hyperpolarized [1-13C]Pyruvate. *Sci. Transl. Med.* **2013**, *5*, 198ra108.

(5) Miloushev, V. Z.; Granlund, K. L.; Boltyanskiy, R.; Lyashchenko, S. K.; DeAngelis, L. M.; Mellinghoff, I. K.; Brennan, C. W.; Tabar, V.; Yang, T. J.; Holodny, A. I.; Sosa, R. E.; Guo, Y. W. W.; Chen, A. P.; Tropp, J.; Robb, F.; Keshari, K. R. Metabolic Imaging of the Human Brain with Hyperpolarized 13C Pyruvate Demonstrates 13C Lactate Production in Brain Tumor Patients. *Cancer Res.* **2018**, *78*, 3755−3760.

(6) Grist, J. T.; McLean, M. A.; Riemer, F.; Schulte, R. F.; Deen, S. S.; Zaccagna, F.; Woitek, R.; Daniels, C. J.; Kaggie, J. D.; Matyz, T.; Patterson, I.; Slough, R.; Gill, A. B.; Chhabra, A.; Eichenberger, R.; Laurent, M.-C.; Comment, A.; Gillard, J. H.; Coles, A. J.; Tyler, D. J.; Wilkinson, I.; Basu, B.; Lomas, D. J.; Graves, M. J.; Brindle, K. M.; Gallagher, F. A. Quantifying Normal Human Brain Metabolism Using Hyperpolarized [1− 13 C]Pyruvate and Magnetic Resonance Imaging. *Neuroimage* **2019**, *189*, 171−179.

(7) Gallagher, F. A.; Woitek, R.; McLean, M. A.; Gill, A. B.; Manzano Garcia, R.; Provenzano, E.; Riemer, F.; Kaggie, J.; Chhabra, A.; Ursprung, S.; Grist, J. T.; Daniels, C. J.; Zaccagna, F.; Laurent, M.-C.; Locke, M.; Hilborne, S.; Frary, A.; Torheim, T.; Boursnell, C.; Schiller, A.; Patterson, I.; Slough, R.; Carmo, B.; Kane, J.; Biggs, H.; Harrison, E.; Deen, S. S.; Patterson, A.; Lanz, T.; Kingsbury, Z.; Ross, M.; Basu, B.; Baird, R.; Lomas, D. J.; Sala, E.; Wason, J.; Rueda, O. M.; Chin, S.-F.; Wilkinson, I. B.; Graves, M. J.; Abraham, J. E.; Gilbert, F. J.; Caldas, C.; Brindle, K. M. Imaging Breast Cancer Using Hyperpolarized Carbon-13 MRI. *Proc. Natl. Acad. Sci. U. S. A.* **2020**, *117*, 2092−2098.

(8) Kurhanewicz, J.; Vigneron, D. B.; Ardenkjaer-Larsen, J. H.; Bankson, J. A.; Brindle, K.; Cunningham, C. H.; Gallagher, F. A.; Keshari, K. R.; Kjaer, A.; Laustsen, C.; Mankoff, D. A.; Merritt, M. E.; Nelson, S. J.; Pauly, J. M.; Lee, P.; Ronen, S.; Tyler, D. J.; Rajan, S. S.; Spielman, D. M.; Wald, L.; Zhang, X.; Malloy, C. R.; Rizi, R. Hyperpolarized 13C MRI: Path to Clinical Translation in Oncology. *Neoplasia.* **2019**, *21*, 1−16.

(9) Mishkovsky, M.; Cheng, T.; Comment, A.; Gruetter, R. Localized in Vivo Hyperpolarization Transfer Sequences. *Magn. Reson. Med.* **2012**, *68*, 349−352.

(10) Larson, P. E. Z.; Chen, H. Y.; Gordon, J. W.; Korn, N.; Maidens, J.; Arcak, M.; Tang, S.; Criekinge, M.; Carvajal, L.; Mammoli, D.; Bok, R.; Aggarwal, R.; Ferrone, M.; Slater, J. B.; Nelson, S. J.; Kurhanewicz, J.; Vigneron, D. B. Investigation of Analysis Methods for Hyperpolarized 13C-Pyruvate Metabolic MRI in Prostate Cancer Patients. *NMR Biomed.* **2018**, *31*, No. e3997.

(11) Laustsen, C.; Østergaard, J. A.; Lauritzen, M. H.; Nørregaard, R.; Bowen, S.; Søgaard, L. V.; Flyvbjerg, A.; Pedersen, M.; Ardenkjær-Larsen, J. H. Assessment of Early Diabetic Renal Changes with Hyperpolarized [1-13C]Pyruvate. *Diabetes/Metab. Res. Rev.* **2013**, *29*, 125−129.

(12) Lewis, A. J. M.; Tyler, D. J.; Rider, O. Clinical Cardiovascular Applications of Hyperpolarized Magnetic Resonance. *Cardiovasc. Drugs Ther.* **2020**, *34*, 231−240.

(13) Grist, J. T.; Miller, J. J.; Zaccagna, F.; McLean, M. A.; Riemer, F.; Matys, T.; Tyler, D. J.; Laustsen, C.; Coles, A. J.; Gallagher, F. A. Hyperpolarized ^{13}C MRI: A Novel Approach for Probing Cerebral Metabolism in Health and Neurological Disease. *J. Cereb. Blood Flow Metab.* **2020**, *21*, 1137−1147.

(14) Chekmenev, E. Y.; Norton, V. A.; Weitekamp, D. P.; Bhattacharya, P. Hyperpolarized 1H NMR Employing Low γ Nucleus for Spin Polarization Storage. *J. Am. Chem. Soc.* **2009**, *131*, 3164−3165.

(15) Truong, M. L.; Coffey, A. M.; Shchepin, R. V.; Waddell, K. W.; Chekmenev, E. Y. Sub-Second Proton Imaging of 13C Hyperpolarized Contrast Agents in Water. *Contrast Media Mol. Imaging* **2014**, *9*, 333−341.

(16) Topping, G. J.; Hundshammer, C.; Nagel, L.; Grashei, M.; Aigner, M.; Skinner, J. G.; Schulte, R. F.; Schilling, F.Acquisition Strategies for Spatially Resolved Magnetic Resonance Detection of Hyperpolarized Nuclei. *Magnetic Resonance Materials in Physics, Biology and Medicine*; Springer April 1, 2020, pp. 221−256. doi: DOI: 10.1007/s10334-019-00807-6.

(17) Sarkar, R.; Comment, A.; Vasos, P. R.; Jannin, S.; Gruetter, R.; Bodenhausen, G.; Hall, H.; Kirik, D.; Denisov, V. P. Proton NMR Of15N-Choline Metabolites Enhanced by Dynamic Nuclear Polarization. *J. Am. Chem. Soc.* **2009**, *131*, 16014−16015.

(18) Morris, G. A.; Freeman, R. Enhancement of Nuclear Magnetic Resonance Signals by Polarization Transfer. *J. Am. Chem. Soc.* **1979**, *101*, 760−762.

(19) Wang, J.; Kreis, F.; Wright, A. J.; Hesketh, R. L.; Levitt, M. H.; Brindle, K. M. Dynamic ^{1}H Imaging of Hyperpolarized [1-^{13}C]Lactate in Vivo Using a Reverse INEPT Experiment. *Magn. Reson. Med.* **2018**, *79*, 741−747.

(20) Feng, Y.; Theis, T.; Liang, X.; Wang, Q.; Zhou, P.; Warren, W. S. Storage of Hydrogen Spin Polarization in Long-Lived 13C 2 Singlet Order and Implications for Hyperpolarized Magnetic Resonance Imaging. *J. Am. Chem. Soc.* **2013**, *135*, 9632−9635.

(21) Theis, T.; Feng, Y.; Wu, T.; Warren, W. S. Composite and Shaped Pulses for Efficient and Robust Pumping of Disconnected Eigenstates in Magnetic Resonance. *J. Chem. Phys.* **2014**, *140*, No. 014201.

(22) Feng, Y.; Theis, T.; Wu, T.-L.; Claytor, K.; Warren, W. S. Long-Lived Polarization Protected by Symmetry. *J. Chem. Phys.* **2014**, *141*, 134307.

(23) Theis, T.; Ortiz, G. X., Jr.; Logan, A. W. J.; Claytor, K. E.; Feng, Y.; Huhn, W. P.; Blum, V.; Malcolmson, S. J.; Chekmenev, E. Y.; Wang, Q.; Warren, W. S. Direct and Cost-Efficient Hyperpolarization of Long-Lived Nuclear Spin States on Universal $^{15}N_2$-Diazirine Molecular Tags. *Sci. Adv.* **2016**, *2*, No. e1501438.

(24) Shen, K.; Logan, A. W. J.; Colell, J. F. P.; Bae, J.; Ortiz, G. X., Jr.; Theis, T.; Warren, W. S.; Malcolmson, S. J.; Wang, Q. Diazirines as Potential Molecular Imaging Tags: Probing the Requirements for Efficient and Long-Lived SABRE-Induced Hyperpolarization. *Am. Ethnol.* **2017**, *129*, 12280−12284.

(25) Bae, J.; Zhou, Z.; Theis, T.; Warren, W. S.; Wang, Q. $^{15}N_4$−1,2,4,5-Tetrazines as Potential Molecular Tags: Integrating Bioorthogonal Chemistry with Hyperpolarization and Unearthing *Para*-N_2. *Sci. Adv.* **2018**, *4*, No. eaar2978.

(26) Zhang, G.; Colell, J. F. P.; Glachet, T.; Lindale, J. R.; Reboul, V.; Theis, T.; Warren, W. S. Terminal Diazirines Enable Reverse

Polarization Transfer from $^{15}N_2$ Singlets. *Am. Ethnol.* **2019**, *131*, 11235−11241.
(27) Roy, S. S.; Rayner, P. J.; Burns, M. J.; Duckett, S. B. A Simple and Cost-Efficient Technique to Generate Hyperpolarized Long-Lived ^{15}N-^{15}N Nuclear Spin Order in a Diazine by Signal Amplification by Reversible Exchange. *J. Chem. Phys.* **2020**, *152*, No. 014201.
(28) Roy, S. S.; Norcott, P.; Rayner, P. J.; Green, G. G. R.; Duckett, S. B. A Hyperpolarizable ^{1}H Magnetic Resonance Probe for Signal Detection 15 Minutes after Spin Polarization Storage. *Am. Ethnol.* **2016**, *128*, 15871−15874.
(29) Tickner, B. J.; Semenova, O.; Iali, W.; Rayner, P. J.; Whitwood, A. C.; Duckett, S. B. Optimisation of Pyruvate Hyperpolarisation Using SABRE by Tuning the Active Magnetisation Transfer Catalyst. *Catal. Sci. Technol.* **2020**, *10*, 1343−1355.
(30) Iali, W.; Roy, S. S.; Tickner, B. J.; Ahwal, F.; Kennerley, A. J.; Duckett, S. B. Hyperpolarising Pyruvate through Signal Amplification by Reversible Exchange (SABRE). *Angew. Chem., Int. Ed.* **2019**, *58*, 10271−10275.
(31) Devience, S. J.; Walsworth, R. L.; Rosen, M. S. Preparation of Nuclear Spin Singlet States Using Spin-Lock Induced Crossing. *Phys. Rev. Lett.* **2013**, *111*, No. 173002.
(32) DeVience, S. J.; Greer, M.; Mandal, S.; Rosen, M. S. Homonuclear J-Coupling Spectroscopy at Low Magnetic Fields Using Spin-Lock Induced Crossing**. *ChemPhysChem* **2021**, *22*, 2128−2137.
(33) Barskiy, D. A.; Kovtunov, K. V.; Koptyug, I. V.; He, P.; Groome, K. A.; Best, Q. A.; Shi, F.; Goodson, B. M.; Shchepin, R. V.; Coffey, A. M.; Waddell, K. W.; Chekmenev, E. Y. The Feasibility of Formation and Kinetics of NMR Signal Amplification by Reversible Exchange (SABRE) at High Magnetic Field (9.4 T). *J. Am. Chem. Soc.* **2014**, *136*, 3322−3325.
(34) Vazquez-Serrano, L. D.; Owens, B. T.; Buriak, J. M. The Search for New Hydrogenation Catalyst Motifs Based on N-Heterocyclic Carbene Ligands. *Inorg. Chim. Acta* **2006**, *359*, 2786−2797.
(35) Cowley, M. J.; Adams, R. W.; Atkinson, K. D.; Cockett, M. C. R.; Duckett, S. B.; Green, G. G. R.; Lohman, J. A. B.; Kerssebaum, R.; Kilgour, D.; Mewis, R. E. Iridium N-Heterocyclic Carbene Complexes as Efficient Catalysts for Magnetization Transfer from Para-Hydrogen. *J. Am. Chem. Soc.* **2011**, *133*, 6134−6137.
(36) Joalland, B.; Nantogma, S.; Chowdhury, M. R. H.; Nikolaou, P.; Chekmenev, E. Y. Magnetic Shielding of Parahydrogen Hyperpolarization Experiments for the Masses. *Magn. Reson. Chem.* **2021**, *59*, 1180−1186.
(37) Nantogma, S.; Joalland, B.; Wilkens, K.; Chekmenev, E. Y. Clinical-Scale Production of Nearly Pure (>98.5%) Parahydrogen and Quantification by Benchtop NMR Spectroscopy. *Anal. Chem.* **2021**, *93*, 3594−3601.
(38) Adelabu, I.; TomHon, P.; Kabir, M. S. H.; Nantogma, S.; Abdulmojeed, M.; Mandzhieva, I.; Ettedgui, J.; Swenson, R. E.; Krishna, M. C.; Theis, T.; Goodson, B. M.; Chekmenev, E. Y. Order-Unity ^{13}C Nuclear Polarization of [1-^{13}C]Pyruvate in Seconds and the Interplay of Water and SABRE Enhancement. *ChemPhysChem* **2022**, *23*, No. e202100839.
(39) Tomhon, P.; Abdulmojeed, M.; Adelabu, I.; Nantogma, S.; Shah, M.; Kabir, H.; Lehmkuhl, S.; Chekmenev, E. Y.; Theis, T.Temperature Cycling Enables Efficient ^{13}C SABRE-SHEATH Hyperpolar-Ization and Imaging of [1−^{13}C]Pyruvate. *J. Am. Chem. Soc.* , *144* (), 282−287, DOI: 10.1021/jacs.1c09581.
(40) Coffey, A. M.; Truong, M. L.; Chekmenev, E. Y. Low-Field MRI Can Be More Sensitive than High-Field MRI. *J. Magn. Reson.* **2013**, *237*, 169−174.
(41) Ariyasingha, N. M.; Lindale, J. R.; Eriksson, S. L.; Clark, G. P.; Theis, T.; Shchepin, R. V.; Chukanov, N. V.; Kovtunov, K. V.; Koptyug, I. V.; Warren, W. S.; Chekmenev, E. Y. Quasi-Resonance Fluorine-19 Signal Amplification by Reversible Exchange. *J. Phys. Chem. Lett.* **2019**, *10*, 4229−4236.
(42) Theis, T.; Ariyasingha, N. M.; Shchepin, R. V.; Lindale, J. R.; Warren, W. S.; Chekmenev, E. Y. Quasi-Resonance Signal Amplification by Reversible Exchange. *J. Phys. Chem. Lett.* **2018**, *9*, 6136−6142.
(43) Hogben, H. J.; Krzystyniak, M.; Charnock, G. T. P.; Hore, P. J.; Kuprov, I. Spinach - A Software Library for Simulation of Spin Dynamics in Large Spin Systems. *J. Magn. Reson.* **2011**, *208*, 179−194.
(44) Shchepin, R. V.; Truong, M. L.; Theis, T.; Coffey, A. M.; Shi, F.; Waddell, K. W.; Warren, W. S.; Goodson, B. M.; Chekmenev, E. Y. Hyperpolarization of "Neat" Liquids by NMR Signal Amplification by Reversible Exchange. *J. Phys. Chem. Lett.* **2015**, *6*, 1961−1967.
(45) Coffey, A. M.; Kovtunov, K. V.; Barskiy, D. A.; Koptyug, I. V.; Shchepin, R. V.; Waddell, K. W.; He, P.; Groome, K. A.; Best, Q. A.; Shi, F.; Goodson, B. M.; Chekmenev, E. Y. High-Resolution Low-Field Molecular Magnetic Resonance Imaging of Hyperpolarized Liquids. *Anal. Chem.* **2014**, *86*, 9042−9049.
(46) Truong, M. L.; Theis, T.; Coffey, A. M.; Shchepin, R. V.; Waddell, K. W.; Shi, F.; Goodson, B. M.; Warren, W. S.; Chekmenev, E. Y. 15N Hyperpolarization by Reversible Exchange Using SABRE-SHEATH. *J. Phys. Chem. C* **2015**, *119*, 8786−8797.
(47) Theis, T.; Truong, M. L.; Coffey, A. M.; Shchepin, R. V.; Waddell, K. W.; Shi, F.; Goodson, B. M.; Warren, W. S.; Chekmenev, E. Y. Microtesla SABRE Enables 10% Nitrogen-15 Nuclear Spin Polarization. *J. Am. Chem. Soc.* **2015**, *137*, 1404−1407.
(48) Levitt, M. H. Symmetry Constraints on Spin Dynamics: Application to Hyperpolarized NMR. *J. Magn. Reson.* **2016**, *262*, 91−99.
(49) Pileio, G.; Carravetta, M.; Levitt, M. H. Storage of Nuclear Magnetization as Long-Lived Singlet Order in Low Magnetic Field. *Proc. Natl. Acad. Sci. U. S. A.* **2010**, *107*, 17135−17139.

https://doi.org/10.1021/acssensors.2c01608
ACS Sens. 2022, 7, 3773−3781